RSC Advances

PAPER

View Article Online
View Journal | View Issue

Check for updates

Cite this: *RSC Adv.*, 2022, **12**, 29709

Degradation of sulfamethoxazole in water by $AgNbO_3$ photocatalyst mediated by persulfate

Chung-Shin Lu, *[a] Hwei-Yan Tsai,[bc] Janah Shaya,[de] Vladimir B. Golovko,[f] Syuan-Yun Wang,[b] Wen-Jin Liu[g] and Chiing-Chang Chen*[g]

In this paper, silver niobate ($AgNbO_3$) material was synthesized by a solid-state reaction. $AgNbO_3$ was characterized using X-ray diffraction (XRD), scanning electron microscopy (SEM), X-ray photoelectron spectroscopy (XPS), UV-visible diffuse reflectance spectroscopy (DRS), and Brunauer–Emmett–Teller (BET) measurement. The photocatalytic activity of $AgNbO_3$ was investigated in degradation of sulfamethoxazole (SMX) under visible light, which is a widely used antibiotic with significant threats towards health and aquatic organisms. Persulfate (PS) oxidant was found to improve the efficiency of the proposed photocatalytic removal of SMX by $AgNbO_3$. The different operational parameters in the $AgNbO_3$/PS/Vis system were investigated. The best photocatalytic performance was achieved with 0.5 g L^{-1} $AgNbO_3$, 1.0 mM PS, and pH = 5.0 as the optimal conditions, achieving 98% of SMX degradation after 8 h of visible-light irradiation. Scavenger and electron spin resonance (ESR) experiments were carried out to identify the major reactive species in the SMX degradation and to propose the photocatalytic mechanism by the $AgNbO_3$/PS/Vis system. The photodecomposition was found to be majorly caused by holes and $^{\bullet}O_2^-$ species, with $^{\bullet}OH$ and $SO_4^{\bullet-}$ radicals contributing to improve the photocatalytic process. The $AgNbO_3$ catalyst was stable and reusable with efficient photocatalytic activity in three successive recycling experiments and its XRD patterns remained virtually unchanged. The reported process of PS activation by the $AgNbO_3$ photocatalyst is promising for visible-light application in remediation of antibiotic-contaminated water.

Received 1st June 2022
Accepted 10th October 2022

DOI: 10.1039/d2ra03408e

rsc.li/rsc-advances

Open Access Article. Published on 17 October 2022. Downloaded on 7/30/2025 7:05:39 AM.
This article is licensed under a Creative Commons Attribution-NonCommercial 3.0 Unported Licence.

1. Introduction

Pollution caused by the increased use of antibiotics represents a major concern for environmental and water treatment research since they pose significant health threats.[1] Sulfamethoxazole(4-amino-*N*-(5-methyl-3-isoxazolyl)-benzenesulfonamide, SMX) is one of the most widely utilized antibiotics in medicines and feed additives in livestock production.[2] For instance, the total annual consumption of SMX in China was ~313 tons in 2013. SMX was listed among the top 10 high-priority medications in a European review of pharmaceuticals and personal care products.[3–5] In addition to the high-consumption concern, SMX is known for its incomplete metabolization and/or absorption by biological systems in humans and animals. This leads to excretion of considerable amounts of SMX into wastewater systems through urine and feces.[6,7] The widespread use of SMX and the inadequacy of traditional wastewater treatment methods in its complete removal lead to the pervasiveness of this pollutant in aquatic environments. High concentrations of SMX in surface water (0.94 μg L^{-1}) and wastewater treatment effluents (24.8 μg L^{-1}) have been previously reported.[8] Other investigations of the presence of pharmaceuticals in more than 100 river samples from 27 European countries showed the SMX concentration range to be 1 ng L^{-1} to 4.1 μg L^{-1}.[9] Residual SMX is toxic to many aquatic species and causes drug resistance in humans which leads to failure of antibiotic therapy.[10,11] Thus, developing effective treatment methods to limit the presence of SMX in aquatic environments remains an important goal in environmental research.

Several techniques have been investigated for treatment and removal of SMX from water systems such as adsorption, membrane separation, chemical oxidation, and biological treatment.[12–15] None of the studied methods was efficient in removal or treatment of SMX because of its bio-refractory nature

[a]*Department of General Education, National Taichung University of Science and Technology, Taichung 404, Taiwan, Republic of China. E-mail: cslu6@nutc.edu.tw*
[b]*Department of Medical Applied Chemistry, Chung Shan Medical University, Taichung 402, Taiwan, Republic of China*
[c]*Department of Medical Education, Chung Shan Medical University Hospital, Taichung 402, Taiwan, Republic of China*
[d]*College of Medicine and Health Sciences, Khalifa University, Abu Dhabi P.O. Box 127788, United Arab Emirates*
[e]*College of Arts and Sciences, Khalifa University, Abu Dhabi P.O. Box 127788, United Arab Emirates*
[f]*Department of Chemistry, The MacDiarmid Institute for Advanced Materials and Nanotechnology, University of Canterbury, Christchurch 8140, New Zealand*
[g]*Department of Science Education and Application, National Taichung University of Education, Taichung 403, Taiwan, Republic of China*

© 2022 The Author(s). Published by the Royal Society of Chemistry

Open Access Article. Published on 17 October 2022. Downloaded on 7/30/2025 7:05:39 AM.
This article is licensed under a Creative Commons Attribution-NonCommercial 3.0 Unported Licence.

and toxicity at very low concentrations.[11] In comparison to these techniques, photocatalytic degradation of SMX under UV light irradiation has been reported with good results. For instance, TiO_2 photocatalysis showed 30–95% removal of SMX (25–100 mg L^{-1}) under UV light irradiation for 60 min.[16,17] Despite its efficiency, TiO_2 applications in photodecomposition of SMX and other pollutants are still limited since they need UV light for TiO_2 activation. UV light only accounts for 3 to 5% of the solar energy. Therefore, developing visible-light-active photocatalysts is still a major goal for researchers to make photocatalytic water treatment more applicable.

Several reports have shown that niobate-based materials (*e.g.*, Nb_2O_5,[18] $NaNbO_3$,[19] $ZnNb_2O_6$,[20] and $K_4Nb_6O_{17}$ (ref. 21)) exhibit good chemical stability and photocatalytic properties with higher conduction band edge. The wide band energy of these niobate materials (~3.4 eV) and their excitation by UV light also represent major disadvantages in their photocatalytic applications.[22] Among the niobate-based materials, $AgNbO_3$ exhibits a smaller bandgap (~2.8 eV) and strong potential in visible-light driven processes and other applications such as microwave communications and microelectronic technology.[23] Some studies have reported significant visible-light activity of $AgNbO_3$ in O_2 evolution from aqueous $AgNO_3$ solutions[24] and in photodegradation of pollutants such as methyl orange, methyl blue, rhodamine B, and 4-chlorophenol.[25–28]

Previous studies have also demonstrated the benefits of incorporating free radical species such as sulfate and hydroxyl radicals to improve the photocatalytic activity of semiconductors. Sulfate radicals were superior to hydroxyl radicals in photocatalytic applications because of their prolonged lifetime, wide pH range (2–9), and high reactive potential (2.5–3.1 eV).[29–31] Commonly used sources of sulfate radicals are peroxymonosulfate (PMS, HSO_5^-) and persulfate (PS, $S_2O_8^{2-}$). In comparison to PMS, PS is more stable under ambient conditions, less expensive, and is needed in smaller concentrations in degradation applications.[32] Moreover, the end-products generated by PS are sulfate anions, which are not considered as pollutants for their inertness.[33] Different strategies have been investigated to activate PS, such as UV irradiation, heat, and ultrasound.[34–36] Likewise, electron transfer of transition metal ions (*e.g.*, Co^{2+}, Cu^{2+}, Fe^{2+}) is also applied in homogeneous activation processes.[37–39] The latter activation method is limited by a small pH range and the formation of metal sludge.[40] Heterogeneous catalysts such as Co_3O_4, Mn_3O_4, and Fe_3O_4 were thus used to activate PS and overcome these disadvantages.[41–43]

The photocatalytic oxidation performance of $AgNbO_3$ in the presence of PS has not been investigated yet, to the best of our knowledge. In line with our research on photocatalytic water treatment methods,[44–49] this study reports the first investigation of visible-light driven photocatalytic degradation of an organic pollutant (SMX) using $AgNbO_3$/PS system. The major objectives were: (1) synthesizing and characterizing $AgNbO_3$ materials *via* the solid-state reaction; (2) assessing the photocatalytic activity of $AgNbO_3$ in the presence of PS oxidant and finding optimal conditions for SMX degradation ($AgNbO_3$ catalytic dosage, concentration of PS, and initial pH); (3) evaluating the stability and reusability of the $AgNbO_3$ photocatalyst; and (4) understanding the photocatalytic mechanism and the principal active species in the degradation of SMX with the $AgNbO_3$/PS/Vis system.

2. Experimental

2.1. Materials

Sulfamethoxazole (99.7%) was obtained from Sigma-Aldrich and used without additional purification. An aqueous stock solution of SMX (10 mg L^{-1}) was prepared, protected from light, and stored at 4 °C. HPLC analysis was used to confirm the presence of SMX as a pure organic compound. Silver nitrate (99%) and niobium(v) oxide (99.9%) were also obtained from Aldrich and used as the sources of the silver and the niobate in the preparation of the photocatalysts. Potassium persulfate ($K_2S_2O_8$, 99%) was purchased from Panreac and used as the PS source. P25 TiO_2 was obtained from Degussa. Sodium hydroxide, nitric acid, reagent-grade ammonium acetate, and HPLC-grade methanol were purchased from Merck. Water was purified with a Milli-Q water ion-exchange system (Millipore Co.) for a resistivity of 1.8×10^7 Ω cm, and the deionized water was utilized in all the experiments.

2.2. Preparation and characterization of silver niobate

$AgNbO_3$ powders were synthesized using the solid-state reaction method. 2.1 mmol of $AgNO_3$ and 1.0 mmol of Nb_2O_5 were mixed by manual grinding (agate mortar and pestle) for 30 min. The mixture was calcined for 5 h in an alumina crucible at 880 °C. The sample was naturally cooled down to ambient temperature. The impurities were removed by successive treatment with concentrated HNO_3 and H_2O. The final powder was dried for 12 h in an oven at 60 °C.

The composition and phase of the $AgNbO_3$ sample were studied using an X-ray diffractometer (PHILIPS X'PERT Pro MPD). Field-emission scanning electron microscope (FE-SEM, HITACHI S-4800) was used to study the morphology. UV-vis spectrophotometer equipped with an integration sphere (PerkinElmer Lambda 35) was utilized to record the UV-vis diffuse reflectance spectra. The BET specific surface area of the sample was measured with an automatic system (Micromeritics Gemini) using nitrogen gas as the adsorbate, at liquid nitrogen temperature. The binding energy of Ag, Nb, and O were measured at ambient conditions using an X-ray photoelectron spectroscope (XPS, VG Scientific ESCALAB 250). C 1s (284.6 eV) was used to correct the peak position of each element.

2.3. Apparatus and instruments for photocatalytic degradation experiments

The apparatus for the SMX photocatalytic degradation experiments is described elsewhere.[50] The C-75 Chromato-Vue UVP cabinet provided a wide area of illumination from 4 W visible-light tubes positioned on two sides of the cabinet interior. The

© 2022 The Author(s). Published by the Royal Society of Chemistry

Open Access Article. Published on 17 October 2022. Downloaded on 7/30/2025 7:05:39 AM.
This article is licensed under a Creative Commons Attribution-NonCommercial 3.0 Unported Licence.

amount of SMX in the aqueous solution was determined using a Waters LC system, equipped with a binary pump, an auto-sampler, and a photodiode array detector. The electronic spin resonance (ESR) signals of the radicals, trapped by 5,5-dimethyl-1-pyrroline-*N*-oxide (DMPO), were recorded on a Bruker EMX A300-10/12 (Germany) with a microwave bridge (microwave frequency, 9.85 GHz; microwave power, 22.8 mW; modulation frequency, 100 kHz; modulation amplitude, 1 G).

2.4. Procedures and analysis

In each photodegradation experiment, a 100 mL aqueous solution comprising SMX (10 mg L^{-1}) and a certain dosage of $AgNbO_3$ (0.1, 0.25, 0.5, or 1.0 g L^{-1}) were used at a fixed pH value. The initial pH of the solution was adjusted accordingly by adding either HNO_3 or NaOH solution. Each suspension was magnetically stirred in the dark for ~30 min before irradiation in order to ensure achieving an adsorption–desorption equilibrium. An appropriate amount of PS (0.5, 0.75, 1.0, or 1.25 mM) was subsequently added according to each experiment. Irradiation was performed using two fluorescent lamps (F4T5/CW, Philips Lighting Co.), mainly providing visible light in the range of 400–700 nm. The average light intensity striking the surface of the solution was ~1420 lux; measured by a digital luxmeter (XRP-3000 AccuMAX™). At a periodic interval, the suspension was sampled (5 mL) and centrifuged (30 min at 3000 rpm) to separate the $AgNbO_3$ material. The amount of SMX was then quantified using High-Performance Liquid Chromatography (HPLC). The HPLC solvent system was: solvent A: 25 mM aqueous ammonium acetate buffer (pH 6.9), and solvent B: methanol. The flow rate of the mobile phase was programmed at 1 mL min^{-1}. The used linear gradient was: $t = 0$, $A = 95$, $B = 5$; $t = 20$, $A = 50$, $B = 50$; $t = 35$–40, $A = 10$, $B = 90$; and $t = 45$, $A = 95$, $B = 5$. The wavelength used to monitor the elution was 260 nm. Atlantis™ dC_{18} column (250 mm × 4.6 mm i.d., dp = 5 μm) was utilized for the LC analysis. The photocatalytic activity is analyzed using C/C_0 as a function of t (irradiation time), where C and C_0 represent the SMX concentration at a given time and the initial SMX concentration, respectively.

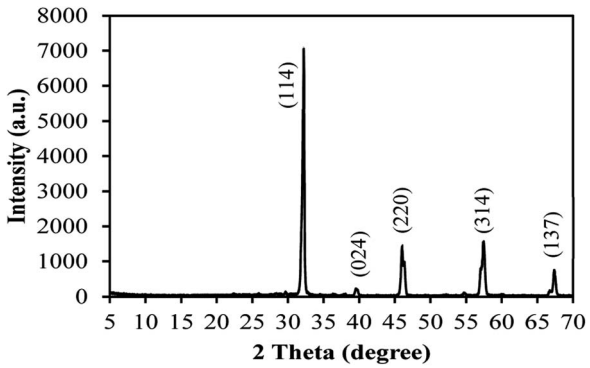

Fig. 1 XRD pattern of the as-prepared $AgNbO_3$ photocatalyst.

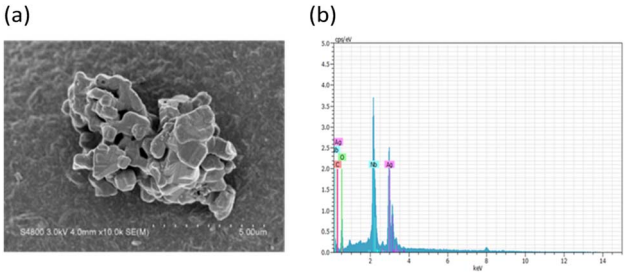

Fig. 2 (a) SEM image and (b) EDS spectrum of the as-prepared $AgNbO_3$ photocatalyst.

3. Results and discussion

3.1. Characterization of silver niobate

The X-ray diffraction pattern of the as-prepared $AgNbO_3$ photocatalyst is displayed in Fig. 1. The diffraction peaks were located at $2\theta = 32.2°$, 39.8°, 46.0°, 57.4°, and 67.4°; corresponding to (1 1 4), (0 2 4), (2 2 0), (3 1 4), and (1 3 7) crystalline planes of cubic phase of $AgNbO_3$ (JCPDS no. 52-0405), respectively.[51,52] No other peaks were observed in the spectrum, attesting for the high purity of the prepared sample. The field-emission SEM image (Fig. 2a) shows the morphology of the powder as clusters of aggregates of smaller $AgNbO_3$ particles formed in irregular stack shapes with a size distribution range of 0.5–1.5 μm. Lastly, the EDS results in Fig. 2b show that silver, niobium, and oxygen are the main elements of the synthesized material.

The photocatalytic activity of a semiconductor is mainly inferred from its optical absorption property, which is relevant to its electronic structure.[53] For this purpose, the UV-vis diffuse reflectance spectrum of the prepared $AgNbO_3$ was recorded (Fig. 3a). The photoabsorption of $AgNbO_3$ was found to span the range from UV to visible light shorter than 450 nm. The steep-edged intense absorption in the visible light region indicates that it originates from band-to-band transition and not from transitions in impurity levels.[54] The band gap energies were estimated using the following relationship: $(\alpha h\nu)^n = k(h\nu - E_g)$. In this equation, α refers to the absorption coefficient, $h\nu$ represents the photonic energy, k is a constant, E_g is the absorption band gap energy, and the value of n is 2 or 0.5 for direct and indirect band gap semiconductors, respectively.[55] The $(\alpha h\nu)^2$ *vs.* $h\nu$ plot of the sample is presented in Fig. 3b. The band gap (E_g) of $AgNbO_3$ was found to be 2.71 eV, which is convenient for photocatalytic degradation of organic contaminants using visible-light irradiation.

The chemical composition and the valence states of the elements in the prepared $AgNbO_3$ powder were further investigated by XPS analysis. The spectra are displayed in Fig. 4, showing the characteristic spin–orbit split signals of Ag $3d_{3/2}$ and Ag $3d_{5/2}$, Nb $3d_{3/2}$ and Nb $3d_{5/2}$, as well as O 1s peak. The two peaks at 367.8 and 373.6 eV in the Ag 3d XPS spectrum (Fig. 4a) correspond to Ag $3d_{5/2}$ and Ag $3d_{3/2}$ of Ag^+, confirming a valence state of +1 for the silver metal. The Nb spectrum

Open Access Article. Published on 17 October 2022. Downloaded on 7/30/2025 7:05:39 AM.
This article is licensed under a Creative Commons Attribution-NonCommercial 3.0 Unported Licence.

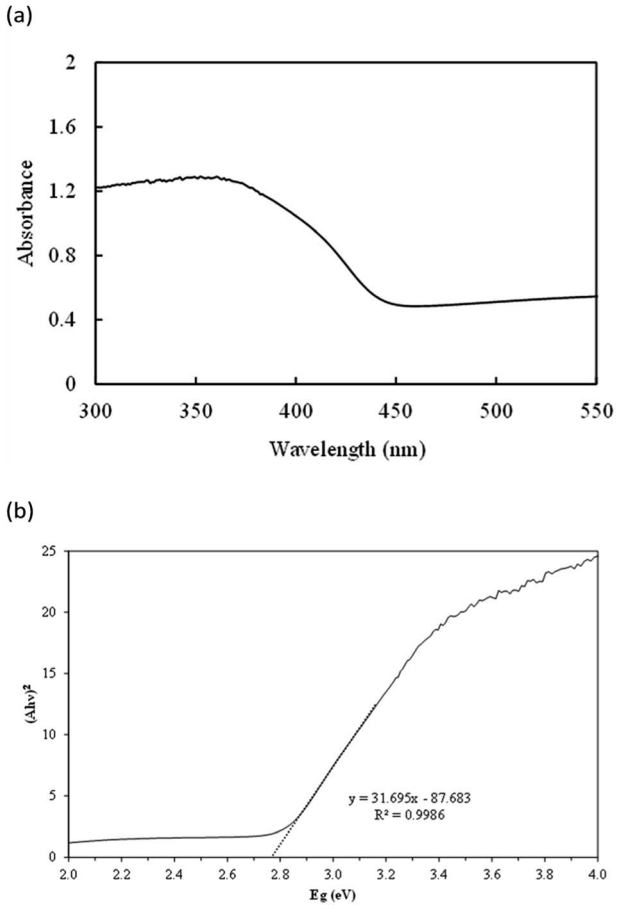

Fig. 3 (a) UV-vis diffuse reflectance spectrum of the as-prepared $AgNbO_3$ photocatalyst; (b) plots of $(\alpha h\nu)^2$ *versus* energy ($h\nu$) for calculating the band gap energy.

(Fig. 4b) shows two peaks at 206.8 and 209.6 eV with 2.8 eV spin–orbit separation, attributed to $3d_{5/2}$ and $3d_{3/2}$ of niobium with +5 valence state. The observed O 1s peak at 529.8 eV (Fig. 4c) is ascribed to the lattice oxygen in the crystalline silver niobate.[56]

Fig. 5 shows the nitrogen adsorption–desorption isotherm of silver niobate. The sample exhibits a type-III isotherm.[57] The BET surface area, pore volume and pore size of the silver niobate sample are 0.52 $m^2\ g^{-1}$, 0.002 $cm^3\ g^{-1}$ and 178.9 nm, respectively.

3.2. Photocatalytic performance

The photocatalytic degradation of SMX was studied to identify the contribution of the $AgNbO_3$ catalyst, PS oxidant, and visible-light irradiation in the process. The results of these experiments are presented in Fig. 6. Under visible-light irradiation only (without $AgNbO_3$ photocatalyst), the concentration of SMX remained almost the same in 12 h, implying that SMX is stable under this photolysis condition. Likewise, only 5% of SMX was degraded under visible-light irradiation for 12 h when PS alone was added to the system, inferring that PS oxidant is not activated by visible light alone. Considering $AgNbO_3$ experiments, ~7% of SMX was removed by adsorption on the silver niobate surface in the dark experiment, and 28% SMX was degraded by $AgNbO_3$ under visible-light irradiation for 12 h. The latter results confirm the photocatalytic role of $AgNbO_3$ in SMX decomposition. The degradation efficiency of SMX was greatly improved when $AgNbO_3$ and PS were used together with visible-light irradiation, achieving almost complete degradation (98%) in 8 h. Thus, PS was an effective oxidant that accelerated the

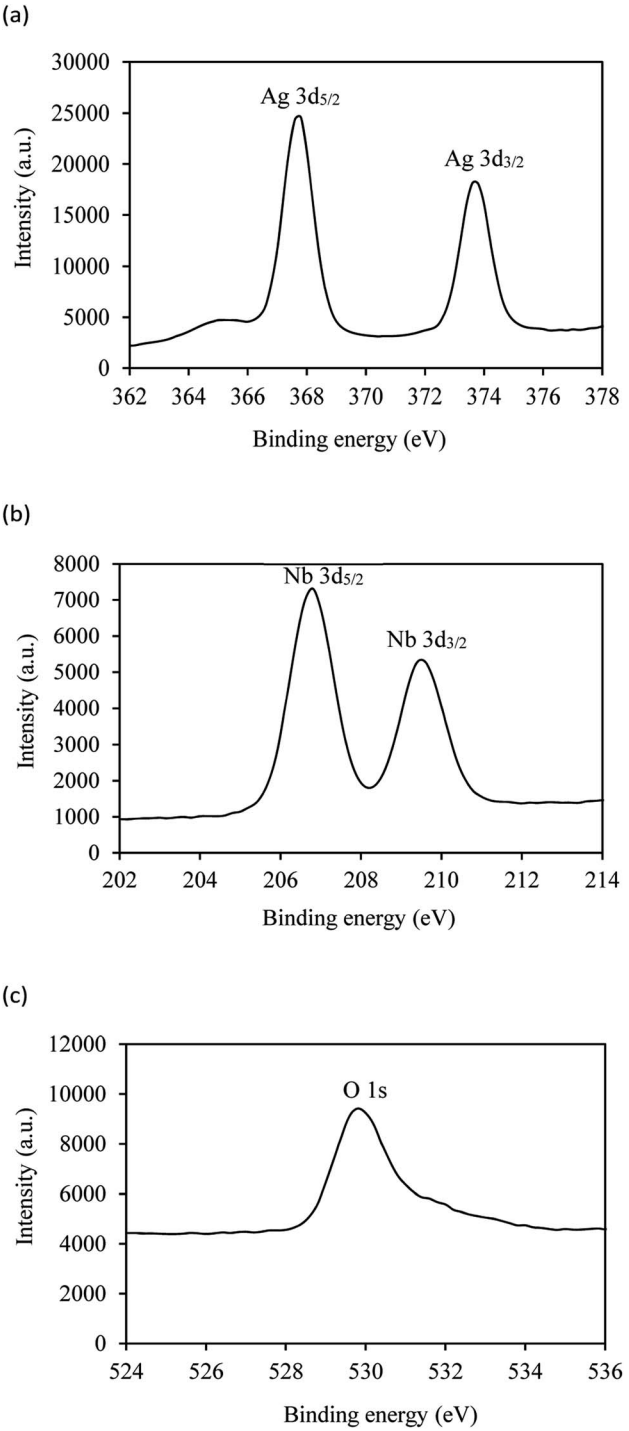

Fig. 4 XPS spectra of the as-prepared $AgNbO_3$ photocatalyst: (a) Ag 3d; (b) Nb 3d; (c) O 1s.

© 2022 The Author(s). Published by the Royal Society of Chemistry

Open Access Article. Published on 17 October 2022. Downloaded on 7/30/2025 7:05:39 AM.
This article is licensed under a Creative Commons Attribution-NonCommercial 3.0 Unported Licence.

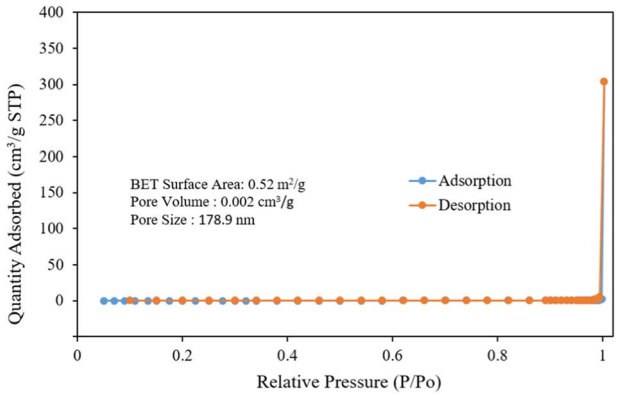

Fig. 5 N_2 adsorption/desorption isotherms of $AgNbO_3$ sample.

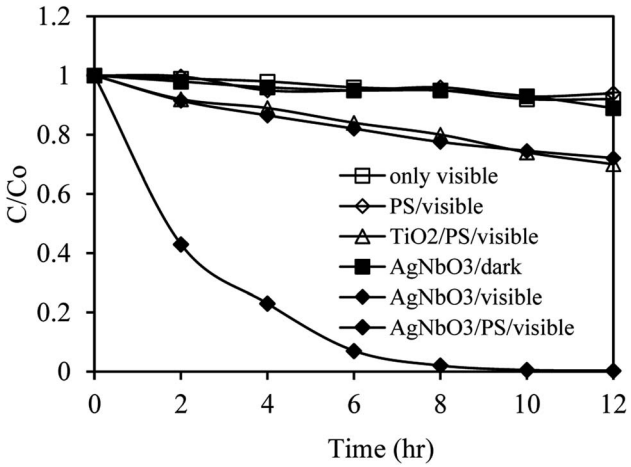

Fig. 6 Comparison of the removal performance using various systems. Unless otherwise stated, the reaction conditions are based on: sulfamethoxazole = 10 mg L^{-1}, catalyst = 0.5 g L^{-1}, PS = 1.0 mM, without pH adjustment.

degradation rate of SMX in the $AgNbO_3$/Vis system by preventing the recombination of the photogenerated electrons and holes and by forming $SO_4^{\bullet -}$ radicals that participate in the oxidation of SMX (eqn (1)–(3)).[58]

$$AgNbO_3 + h\nu \rightarrow h_{VB}^{+} + e_{CB}^{-} \quad (1)$$

$$S_2O_8^{2-} + e_{CB}^{-} \rightarrow SO_4^{\bullet -} + SO_4^{2-} \quad (2)$$

$$SMX + SO_4^{\bullet -} \rightarrow SO_4^{2-} + \text{degradation products of SMX} \quad (3)$$

The photocatalytic performance of the $AgNbO_3$ material was compared to the conventional titanium(IV) oxide semiconductor (TiO_2, P25, 0.5 g L^{-1}) under the same conditions (visible light, PS oxidant, *etc.*). The results of the TiO_2/PS catalytic system (Fig. 6) showed little photocatalytic activity with an SMX degradation rate less than 30% because of TiO_2 needs UV light for activation. In comparison, the $AgNbO_3$/PS system resulted in a degradation rate over 98%, showing an extremely efficient visible-light photocatalytic activity.

3.3. Effects of the catalytic dosage and concentration of the oxidant

The photodegradation of SMX by the $AgNbO_3$/PS/Vis system was optimized by studying various catalytic dosages of $AgNbO_3$, concentrations of the PS oxidant, and initial pH conditions. The employed $AgNbO_3$ catalyst was varied between 0.1 and 1.0 g L^{-1} and the results of the degradation experiments are presented in Fig. 7. SMX removal was negligible in the absence of $AgNbO_3$, as found before. However, increasing the $AgNbO_3$ concentration from 0.1 to 0.5 g L^{-1} enhanced the photodegradation efficiency of SMX from 47% to 98% under visible-light irradiation for 8 h. This enhancement in the photodegradation rates can be attributed to the increase in the accessible catalytic active sites (total surface area) for photocatalytic reactions and PS activation. This results in more effective formation of active radicals.[29,49] 0.5 g L^{-1} was found to be the optimal catalytic dosage after which the photodegradation efficiency of SMX slightly decreased. This decrease might be resulting from scattering of light and reduction of its transmission (shielding effect)

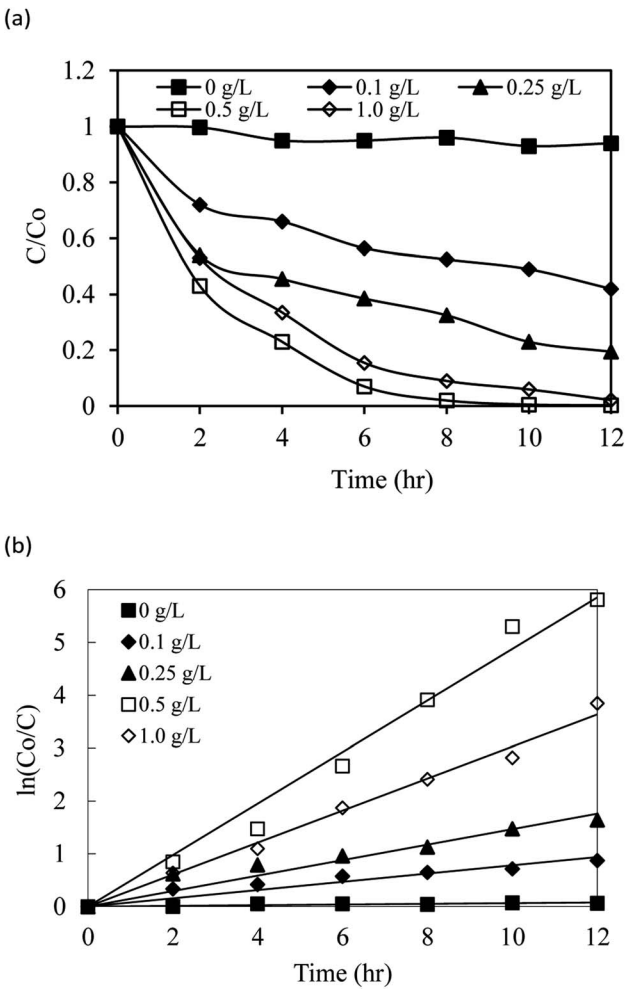

Fig. 7 (a) The effect of $AgNbO_3$ dosage on sulfamethoxazole removal in the $AgNbO_3$/PS/Vis system. Experimental condition: sulfamethoxazole = 10 mg L^{-1}, PS = 1.0 mM, initial pH = 5. (b) Photodegradation kinetics of sulfamethoxazole in the $AgNbO_3$/PS/Vis system.

© 2022 The Author(s). Published by the Royal Society of Chemistry

Open Access Article. Published on 17 October 2022. Downloaded on 7/30/2025 7:05:39 AM.
This article is licensed under a Creative Commons Attribution-NonCommercial 3.0 Unported Licence.

Table 1 Kinetic parameters (rate constants and linear regression coefficients R^2) for photocatalytic degradation of sulfamethoxazole at various catalyst dosages

Catalyst dosage (g L^{-1})	k_{app} (h^{-1})	R^2
0	0.0064	0.9173
0.1	0.0781	0.9735
0.25	0.1467	0.9790
0.5	0.4877	0.9943
1.0	0.3030	0.9968

through the solution because of the increased turbidity and opacity from the excess photocatalyst.[29]

Fig. 7b presents the regression analyses based on the first-order reaction kinetics for the photocatalytic degradation of SMX. The plots of $\ln C_0/C = k_{app}t$ were used to estimate the degradation rate constants (k_{app}) from their slopes (summarized in Table 1 with the linear regression coefficients). The values show that first-order kinetics appear to fit the photodegradation of SMX, and demonstrate that 0.5 g L^{-1} of $AgNbO_3$ is the optimal catalytic dosage. 0.5 g L^{-1} of $AgNbO_3$ was retained in all the experiments that followed.

The results of the SMX degradation experiments with different PS concentrations are presented in Fig. 8. These results demonstrate the significant role of the oxidant concentration in the studied process. It was found that increasing the PS concentration from 0.5 to 1.0 mM improved the photocatalytic degradation efficiency of SMX from 37% to 98% in 8 h. After 1.0 mM, the degradation efficiency was reduced by the increase of PS concentration (1.25 mM). The excess PS can scavenge the active sulfate radicals and compete with their reactions with SMX forming PS radicals ($S_2O_8^{\bullet -}$) with lower reduction potential than that of $SO_4^{\bullet -}$ (eqn (4)), consequently reducing the SMX degradation efficiency.[59] In addition, the increase in the concentration of SO_4^{2-} ion produced from excess PS (eqn (2)) was also reported as a cause for saturation of degradation rates by adsorption on the photocatalytic surface and reduction of accessible catalytic sites.[60] Adsorbed SO_4^{2-} ions might further react with other active species such as $^{\bullet}OH$ radicals (eqn (5)) and photogenerated holes (eqn (6)) forming less active $SO_4^{\bullet -}$ radicals and thus suppressing the degradation rate.

$$S_2O_8^{2-} + SO_4^{\bullet -} \rightarrow SO_4^{2-} + S_2O_8^{\bullet -} \quad (4)$$

$$SO_4^{2-} + {}^{\bullet}OH \rightarrow SO_4^{\bullet -} + OH^- \quad (5)$$

$$SO_4^{2-} + h_{VB}^+ \rightarrow SO_4^{\bullet -} \quad (6)$$

3.4. Effect of initial pH value

The impact of the initial pH value on SMX removal efficiency by $AgNbO_3$/PS/Vis (0.5 g L^{-1}, 10 mg L^{-1}, and 1.0 mM respectively) was studied using acidic (pH = 5), neutral (pH = 7), and alkaline (pH = 9) solutions. The results are depicted in Fig. 9, demonstrating the important effect of pH on the degradation of SMX. When the initial pH was increased from 5 to 9, the degradation efficiency of SMX dropped from 98% to 27% under visible-light irradiation for 8 h. In acidic solutions, $S_2O_8^{2-}$ and the formed $HS_2O_8^-$ (eqn (7)) can easily be adsorbed onto the positively charged $AgNbO_3$ surface. This results in easier generation of the reactive $SO_4^{\bullet -}$ species (eqn (2)) by facilitating the reaction between the photogenerated electron in the conduction band and the persulfate.[33] Alkaline solutions induce the presence of negative charges on the surface of the catalyst, which repel the PS anions. This in turn causes a smaller amount of PS to be activated and decreases the SMX degradation efficiency.[59]

$$S_2O_8^{2-} + H^+ \rightarrow HS_2O_8^- \; K < 0.05 \quad (7)$$

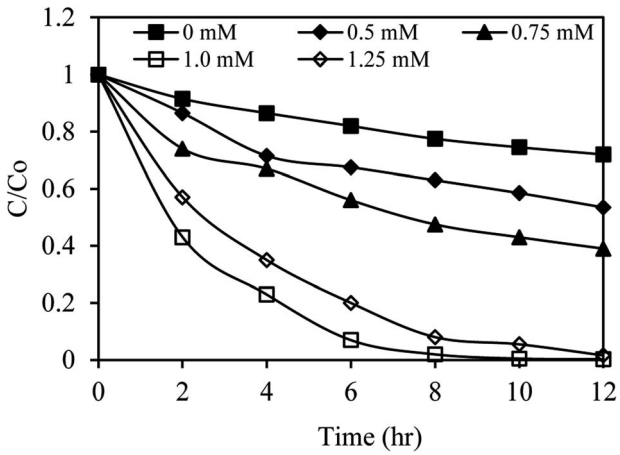

Fig. 8 The effect of PS concentration on sulfamethoxazole removal in the $AgNbO_3$/PS/Vis system. Experimental conditions: sulfamethoxazole = 10 mg L^{-1}, catalyst = 0.5 g L^{-1}, initial pH = 5.

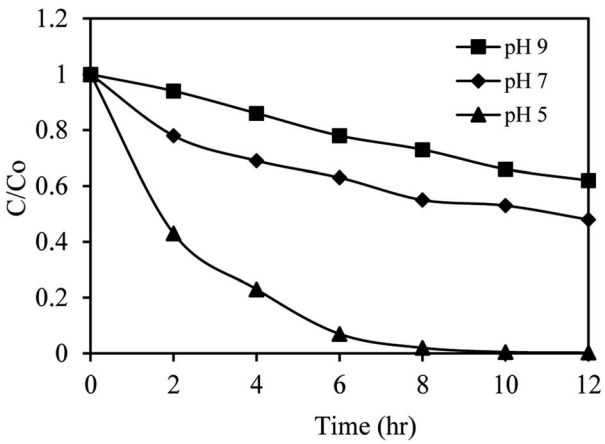

Fig. 9 The effect of initial pH on sulfamethoxazole removal in the $AgNbO_3$/PS/Vis system. Experimental condition: sulfamethoxazole = 10 mg L^{-1}, catalyst = 0.5 g L^{-1}, PS = 1.0 mM.

© 2022 The Author(s). Published by the Royal Society of Chemistry

Open Access Article. Published on 17 October 2022. Downloaded on 7/30/2025 7:05:39 AM.
This article is licensed under a Creative Commons Attribution-NonCommercial 3.0 Unported Licence.

3.5. Active species in photodegradation of SMX

Quenching studies and ESR measurements were used to identify the major reactive radical species in the photocatalytic decomposition of SMX by the $AgNbO_3$/PS/Vis system. Methanol (MeOH) was used to quench $SO_4^{\bullet-}$ ($k = 2.5 \times 10^7$ M^{-1} s^{-1}) and $^{\bullet}OH$ ($k = 9.7 \times 10^8$ M^{-1} s^{-1}) radicals. *tert*-Butyl alcohol (TBA) was added as a more selective scavenger for the $^{\bullet}OH$ radicals. The rate constant of the latter with $^{\bullet}OH$ is 3.8–7.6 $\times$ 10^8 M^{-1} s^{-1}, ~1000-fold faster than its reaction with $SO_4^{\bullet-}$ species (k = 4.0–9.1 $\times$ 10^5 M^{-1} s^{-1}).[29] Ammonium oxalate (AO), benzoquinone (BQ), and sodium azide (SA) were used to scavenge the h^+, $^{\bullet}O_2^-$, and $^1O_2$ potential active species, respectively.[49,61] Fig. 10 displays the SMX degradation efficiency with the $AgNbO_3$/PS/Vis system in the presence and absence of scavengers. Compared to the control experiment without any scavenger, AO (1 mM) strongly reduced the degradation efficiency from 98% to 26% in 8 h, inferring the significant role of h^+ in the studied degradation. BQ (1 mM) showed a comparable inhibition to 45%, indicating that $^{\bullet}O_2^-$ radicals participate in the degradation reaction. A negligible change was obtained in the degradation efficiencies when SA was added. This shows that $^1O_2$ species plays a less important role in the photocatalytic degradation of SMX. Fig. 10b shows that low concentrations (1 mM) of TBA and MeOH induced much smaller inhibition of the degradation process to 92% and 74% in 8 h, respectively. Increasing the respective concentrations of the latter scavengers to 100 mM further inhibited the rates to 68% and 48% in 8 h. It can be concluded that $^{\bullet}OH$ and $SO_4^{\bullet-}$ radicals contribute to the tested photocatalytic process that is mainly driven by the holes and $^{\bullet}O_2^-$ species.

The ESR spin-trap technique (with 5,5-dimethylpyridine-*N*-oxide (DMPO)) was further employed to identify the generated radicals in SMX degradation by the $AgNbO_3$/PS/Vis system (Fig. 11). No ESR signal was found in the dark experiment.

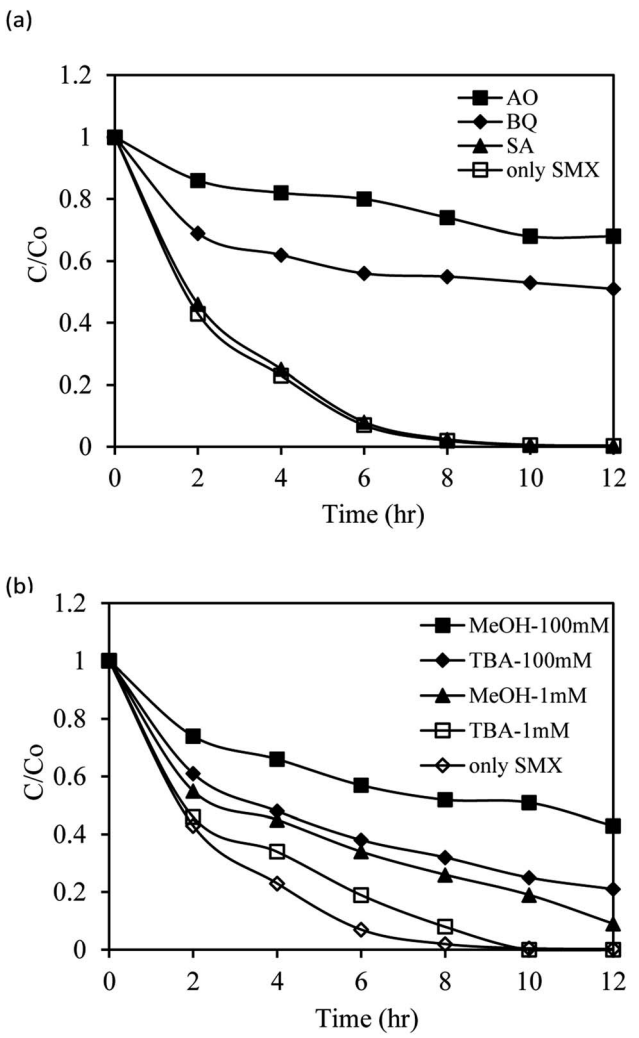

Fig. 10 Photocatalytic degradation of sulfamethoxazole with $AgNbO_3$/PS/Vis in the absence and presence of scavengers (AO, BQ, SA, MeOH and TBA) under visible-light irradiation.

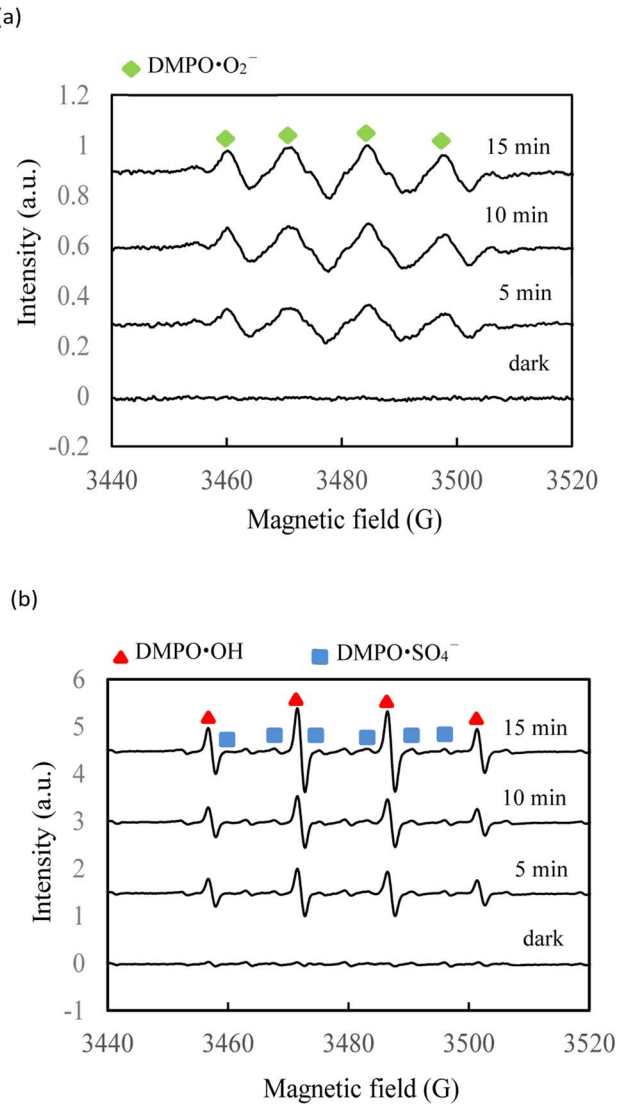

Fig. 11 5,5-Dimethylpyridine-*N*-oxide (DMPO) spin-trapping ESR spectra for DMPO-$^{\bullet}O_2^-$, DMPO-$^{\bullet}OH$ and DMPO-$^{\bullet}SO_4^-$ under visible-light irradiation with $AgNbO_3$/PS/Vis. (a) DMPO-$^{\bullet}O_2^-$ (b) DMPO-$^{\bullet}OH$ and DMPO-$^{\bullet}SO_4^-$.

© 2022 The Author(s). Published by the Royal Society of Chemistry

Open Access Article. Published on 17 October 2022. Downloaded on 7/30/2025 7:05:39 AM.
This article is licensed under a Creative Commons Attribution-NonCommercial 3.0 Unported Licence.

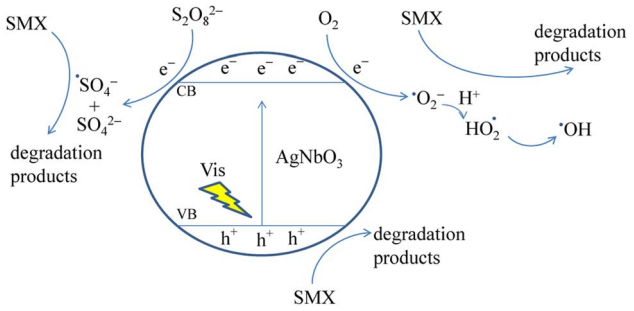

Fig. 12 Schematic diagram illustrating the photocatalytic mechanism of the $AgNbO_3$/PS/Vis system.

Under visible-light irradiation, characteristic signals of reactive oxygen species were observed showing the photoactivation of the $AgNbO_3$ catalyst. Signals for DMPO-$^{\bullet}O_2^-$ (intensity ratios of 1 : 1 : 1 : 1) and DMPO-$^{\bullet}OH$ (intensity ratios of 1 : 2 : 2 : 1) spin adducts clearly appeared.[29] In addition, DMPO-$^{\bullet}SO_4^-$ signals were identified in the $AgNbO_3$/PS/Vis catalytic process. The ESR results are in accordance with the results of the scavenger experiments.

The mechanism of the photocatalytic degradation of SMX by the $AgNbO_3$/PS/Vis system is proposed in Fig. 12 based on the findings in this study. Upon photoexcitation by visible light, electrons from the valence band (VB) of the $AgNbO_3$ catalyst are promoted to the conduction band (CB), forming holes (h_{VB}^+) and free electrons (e_{CB}^-) on the surface of the catalyst. The holes have strong oxidizing power and can directly participate in oxidation of the SMX molecules. The free electrons can react with molecular oxygen in the solution and form $^{\bullet}O_2^-$ and $^{\bullet}OH$ active radicals.[48] The oxidative holes and the active oxygen radicals attack the organic pollutants and degrade them gradually. The addition of PS to the reaction system improved the separation efficiency of the photogenerated charge carriers and slowed the rate of their recombination. Moreover, PS acted as an acceptor for the photogenerated electrons forming reactive $SO_4^{\bullet-}$ and $^{\bullet}OH$ species for SMX oxidation.[62,63] In sum, incorporating the PS oxidant to the $AgNbO_3$/Vis system significantly improved the SMX degradation efficiency.

3.6. Efficiency of the catalytic system in recycling experiments

Practical photocatalytic applications depend on the stability of the photocatalyst. The stability and efficiency of the $AgNbO_3$/PS/Vis catalytic system were hence assessed in 3 successive recycling experiments of SMX removal. After each run, the $AgNbO_3$ material was collected from the solution, dried, and reutilized in the next photocatalytic experiment under the same conditions. The results (Fig. 13a) show the stability and reusability of the $AgNbO_3$ catalyst in SMX degradation with a small reduction of its photocatalytic activity to 82% in the third run. This is due to the inevitable loss of the $AgNbO_3$ in the recycling and sampling of SMX aliquots for analysis. The stability is further evidenced by the insignificant change in the XRD patterns of the fresh and reused $AgNbO_3$ catalysts (Fig. 13b). The same

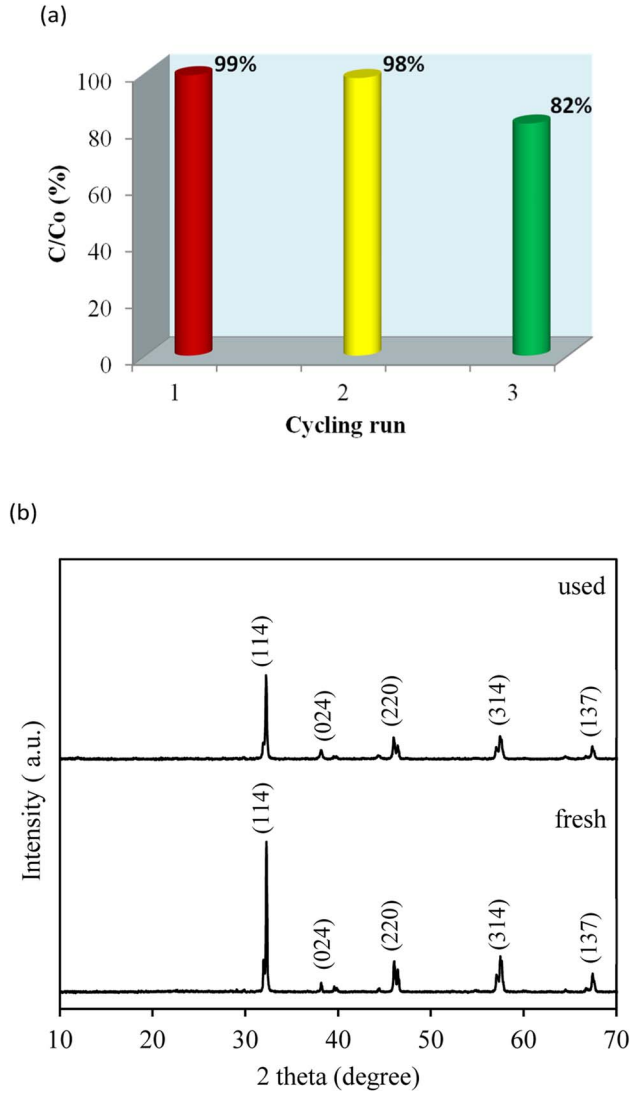

Fig. 13 (a) Cycling runs and (b) XRD patterns acquired before and after the photocatalytic degradation of sulfamethoxazole in the presence of $AgNbO_3$ (0.5 g L^{-1}) and PS (1.0 mM) under visible-light irradiation.

characteristic peaks of (1 1 4), (0 2 4), (2 2 0), (3 1 4), and (1 3 7) planes of standard XRD JCPDS card for $AgNbO_3$ were observed.[51,52] The present investigation favor the efficient long-term application of the $AgNbO_3$/PS/Vis catalytic system in SMX removal and water treatment without photocorrosion.

4. Conclusions

A catalytic system consisting of $AgNbO_3$ material and PS oxidant was proposed for photocatalytic degradation of sulfamethoxazole under visible-light irradiation. PS was found to be an efficient oxidant that significantly accelerates the $AgNbO_3$/Vis system and improves its photocatalytic performance for SMX degradation. The optimal conditions for the proposed SMX removal method were investigated. The photodegradation rate increased with increasing the catalyst dosage to 0.5 g L^{-1} and with increasing the PS concentration to 1.0 mM as optimal

© 2022 The Author(s). Published by the Royal Society of Chemistry

Open Access Article. Published on 17 October 2022. Downloaded on 7/30/2025 7:05:39 AM.
This article is licensed under a Creative Commons Attribution-NonCommercial 3.0 Unported Licence.

conditions. Acidic solutions were found to be more suitable for SMX degradation by the studied system. The degradation rates were reduced considerably in neutral and alkaline solutions. Photogenerated holes and $^{\bullet}O_2^-$ radicals were the major reactive species in the process, with some contributions from other radicals such as $^{\bullet}OH$ and $SO_4^{\bullet-}$. The $AgNbO_3$ catalyst demonstrated its stability and reusability in recycling experiments without noticeable changes in its XRD patterns upon its use in photodecomposition of SMX. The chemical stability and durable photocatalytic activity of the $AgNbO_3$ material as well as the efficiency of $AgNbO_3$/PS/Vis system in SMX degradation show its potential in wastewater treatment applications.

Conflicts of interest

There is no conflict to declare.

Acknowledgements

This research was supported by the Ministry of Science and Technology of the Republic of China (MOST 110-2637-M-025-001). We thank the Instrumentation Center of Chung Hsing University, Taiwan (FA05B101X), Instrumentation Center at National Tsing Hua University, Taiwan (FA04B101X), and Precious Instrument Utilization Center at National Central University, Taiwan (FA07B101X) for utilization of precious instrument.

References

1 M. Xu, J. Deng, A. Cai, X. Ma, J. Li, Q. Li and X. Li, *Chem. Eng. J.*, 2020, **384**, 123320.
2 Y. Ji, Y. Fan, K. Liu, D. Kong and J. Lu, *Water Res.*, 2015, **87**, 1–9.
3 J. Guo, Y. Zhang, J. Mo, H. Sun and Q. Li, *Front. Microbiol.*, 2021, **12**, 541451.
4 D. J. Jasim and A. K. Abbas, *Eurasian Chem. Commun.*, 2022, **4**, 16–40.
5 Q.-Q. Zhang, G.-G. Ying, C.-G. Pan, Y.-S. Liu and J.-L. Zhao, *Environ. Sci. Technol.*, 2015, **49**, 6772–6782.
6 A. K. Sarmah, M. T. Meyer and A. B. Boxall, *Chemosphere*, 2006, **65**, 725–759.
7 W. Tappe, M. Herbst, D. Hofmann, S. Koeppchen, S. Kummer, B. Thiele and J. Groeneweg, *Appl. Environ. Microbiol.*, 2013, **79**, 2572–2577.
8 S. Gao, Z. Zhao, Y. Xu, J. Tian, H. Qi, W. Lin and F. Cui, *J. Hazard. Mater.*, 2014, **274**, 258–269.
9 R. Loos, B. M. Gawlik, G. Locoro, E. Rimaviciute, S. Contini and G. Bidoglio, *Environ. Pollut.*, 2009, **157**, 561–568.
10 J. Yang, Z. Li and H. Zhu, *Appl. Catal., B*, 2017, **217**, 603–614.
11 J. R. Kim and E. Kan, *J. Environ. Manage.*, 2016, **180**, 94–101.
12 Q. Li, W. Yu, L. Guo, Y. Wang, S. Zhao, L. Zhou and X. Jiang, *Materials*, 2021, **14**, 1033.
13 W. Q. Guo, R. L. Yin, X. J. Zhou, J. S. Du, H. O. Cao, S. S. Yang and N. Q. Ren, *Ultrason. Sonochem.*, 2015, **22**, 182–187.
14 J. L. Tambosi, R. F. de Sena, M. Favier, W. Gebhardt, H. J. José, H. F. Schröder and R. d. F. P. M. Moreira, *Desalination*, 2010, **261**, 148–156.
15 X.-l. Guo, Z.-w. Zhu and H.-l. Li, *J. Mol. Liq.*, 2014, **198**, 169–172.
16 M. N. Abellán, B. Bayarri, J. Giménez and J. Costa, *Appl. Catal., B*, 2007, **74**, 233–241.
17 L. Hu, P. M. Flanders, P. L. Miller and T. J. Strathmann, *Water Res.*, 2007, **41**, 2612–2626.
18 F. Huang, H. Zhao, A. Yan, Z. Li, H. Liang, Q. Gao and Y. Qiang, *J. Alloys Compd.*, 2017, **695**, 489–495.
19 L. Wang, H. Gu, J. He, T. Zhao, X. Zhang, C. Xiao, H. Liu, X. Zhang and Y. Li, *J. Alloys Compd.*, 2017, **695**, 599–606.
20 Y. Chun, M. Yue, P. Jiang, S. Chen, W. Gao, R. Cong and T. Yang, *RSC Adv.*, 2018, **8**, 13857–13864.
21 C. Zhou, G. Chen and Q. Wang, *J. Mol. Catal. A: Chem.*, 2011, **339**, 37–42.
22 X. Liu, C. Qin, L. Cao, Y. Feng, Y. Huang, L. Qin and H. J. Seo, *J. Alloys Compd.*, 2017, **724**, 381–388.
23 L. Yang, J. Liu, H. Chang and S. Tang, *RSC Adv.*, 2015, **5**, 59970–59975.
24 H. Kato, H. Kobayashi and A. Kudo, *J. Phys. Chem. B*, 2002, **106**, 12441–12447.
25 W. Wu, S. Liang, Y. Chen, L. Shen, R. Yuan and L. Wu, *Mater. Res. Bull.*, 2013, **48**, 1618–1626.
26 L. Cao, Z. Guo, J. Huang, C. Li, J. Fei, Q. Feng, P. Wen, Y. Sun and X. Kong, *Mater. Lett.*, 2014, **137**, 110–112.
27 W. Wang, G. Li, Y. Bai, N. Yang and W. Zhang, *J. Phys. Chem. Solids*, 2011, **72**, 1457–1461.
28 Y. Lu, Q. Yu, F. Zhang, G. Li and W. Zhang, *Appl. Phys. A: Mater. Sci. Process.*, 2016, **122**, 850.
29 C. C. Chen, H. J. Fan, J. Shaya, Y. K. Chang, V. B. Golovko, O. Toulemonde, C. H. Huang, Y. X. Song and C. S. Lu, *Appl. Organomet. Chem.*, 2019, **33**, e5113.
30 Y. Yang, J. Jiang, X. Lu, J. Ma and Y. Liu, *Environ. Sci. Technol.*, 2015, **49**, 7330–7339.
31 P. Shukla, I. Fatimah, S. Wang, H. M. Ang and M. O. Tadé, *Catal. Today*, 2010, **157**, 410–414.
32 C. Wang, S. Jia, Y. Zhang, Y. Nian, Y. Wang, Y. Han, Y. Liu, H. Ren, S. Wu, K. Yao and X. Han, *Appl. Catal., B*, 2020, **270**, 118819.
33 R. Hazime, Q. H. Nguyen, C. Ferronato, A. Salvador, F. Jaber and J. M. Chovelon, *Appl. Catal., B*, 2014, **144**, 286–291.
34 J. Guo, L. Zhu, N. Sun and Y. Lan, *J. Taiwan Inst. Chem. Eng.*, 2017, **78**, 137–143.
35 S. A. Kordkandi and M. Forouzesh, *J. Taiwan Inst. Chem. Eng.*, 2014, **45**, 2597–2604.
36 G. P. Anipsitakis and D. D. Dionysiou, *Environ. Sci. Technol.*, 2004, **38**, 3705–3712.
37 P. Gayathri, R. Praveena Juliya Dorathi and K. Palanivelu, *Ultrason. Sonochem.*, 2010, **17**, 566–571.
38 H.-y. Liang, Y.-q. Zhang, S.-b. Huang and I. Hussain, *Chem. Eng. J.*, 2013, **218**, 384–391.
39 J. Wu, H. Zhang and J. Qiu, *J. Hazard. Mater.*, 2012, **215–216**, 138–145.
40 F. Liu, Y. Xu, B. Zhang, Y. Liu and H. Zhang, *Chemosphere*, 2020, **238**, 124611.

© 2022 The Author(s). Published by the Royal Society of Chemistry

Open Access Article. Published on 17 October 2022. Downloaded on 7/30/2025 7:05:39 AM.
This article is licensed under a Creative Commons Attribution-NonCommercial 3.0 Unported Licence.

41 H. Lin, H. Zhang and L. Hou, *J. Hazard. Mater.*, 2014, **276**, 182–191.
42 D. Ouyang, J. Yan, L. Qian, Y. Chen, L. Han, A. Su, W. Zhang, H. Ni and M. Chen, *Chemosphere*, 2017, **184**, 609–617.
43 E. Saputra, S. Muhammad, H. Sun, H. M. Ang, M. O. Tade and S. Wang, *J. Colloid Interface Sci.*, 2013, **407**, 467–473.
44 C.-C. Chen, S.-H. Chang, J. Shaya, F.-Y. Liu, Y.-Y. Lin, L.-G. Wang, H.-Y. Tsai and C.-S. Lu, *J. Taiwan Inst. Chem. Eng.*, 2022, **133**, 104272.
45 C.-C. Chen, T.-T. Chen, J. Shaya, C.-L. Wu and C.-S. Lu, *J. Taiwan Inst. Chem. Eng.*, 2021, **123**, 228–244.
46 C. C. Chen, J. Shaya, K. Polychronopoulou, V. B. Golovko, S. Tesana, S. Y. Wang and C. S. Lu, *Nanomaterials*, 2021, **11**, 1325.
47 H. Tsai, J. Shaya, S. Tesana, V. B. Golovko, S.-Y. Wang, Y.-Y. Liao, C.-S. Lu and C.-C. Chen, *Catalysts*, 2020, **10**, 857.
48 C.-C. Chen, J. Shaya, H.-J. Fan, Y.-K. Chang, H.-T. Chi and C.-S. Lu, *Sep. Purif. Technol.*, 2018, **206**, 226–238.
49 S. Huang, C. Chen, H. Tsai, J. Shaya and C. Lu, *Sep. Purif. Technol.*, 2018, **197**, 147–155.
50 C. C. Chen, C. S. Lu, F. D. Mai and C. S. Weng, *J. Hazard. Mater.*, 2006, **137**, 1600–1607.
51 M. Yang, Y. Pu, W. Wang, J. Li, X. Guo, R. Shi and Y. Shi, *J. Alloys Compd.*, 2019, **811**, 151831.
52 P. Chen, P. Xing, Z. Chen, X. Hu, H. Lin, L. Zhao and Y. He, *J. Colloid Interface Sci.*, 2019, **534**, 163–171.
53 J. Tang, Z. Zou and J. Ye, *Angew. Chem., Int. Ed.*, 2004, **43**, 4463–4466.
54 A. Kudo, H. Kato and I. Tsuji, *Chem. Lett.*, 2004, **33**, 1534–1539.
55 L. Wang, X. Li, W. Teng, Q. Zhao, Y. Shi, R. Yue and Y. Chen, *J. Hazard. Mater.*, 2013, **244–245**, 681–688.
56 X. Kong, Z. Guo, Q. Lu, J. Huang, L. Cao, L. Yin, J. Li and Q. Feng, *J. Alloys Compd.*, 2016, **686**, 48–54.
57 S. J. Gregg and K. S. W. Sing, *Adsorption surface area and porosity*, Academic Press. London, 1982, pp.3–12.
58 S. Yamazaki, T. Mori, T. Katou, M. Sugihara, A. Saeki and T. Tanimura, *J. Photochem. Photobiol., A*, 2008, **199**, 330–335.
59 M. Ahmadi, F. Ghanbari and M. Moradi, *Water Sci. Technol.*, 2015, **72**, 2095–2102.
60 A. Syoufian and K. Nakashima, *J. Colloid Interface Sci.*, 2007, **313**, 213–218.
61 R. Wang, M. Shi, F. Xu, Y. Qiu, P. Zhang, K. Shen, Q. Zhao, J. Yu and Y. Zhang, *Nat. Commun.*, 2020, **11**, 4465.
62 D. Tian, H. Zhou, H. Zhang, P. Zhou, J. You, G. Yao, Z. Pan, Y. Liu and B. Lai, *Chem. Eng. J.*, 2022, **428**, 131166.
63 J. Gong, J. Zhang, H. Lin and J. Yuan, *Appl. Mater. Today*, 2018, **12**, 168–176.

© 2022 The Author(s). Published by the Royal Society of Chemistry